Theoretical Considerations in Designing Ultra-High Speed All-Optical Clock Recovery Using Fiber Optical Parametric Amplifiers

Rasoul Damani and Jawad A. Salehi, *Fellow, IEEE*

***Abstract*—In this paper, a new all-optical phase-locked loop (OPLL) in a TDM system is proposed and analyzed. The scheme relies on using fiber optical parametric amplifier (FOPA) device models and theories. In the proposed OPLL, the local clock pulse stream and the received data signal pulses are fed into the FOPA as its pump and amplified signals, respectively. The power of the resulting, relatively, strong *idler* signal depends on the phase difference between the local clock and the received data signal pulses, and it is used to reveal the OPLL's error signal. We characterize the mathematical structure of the proposed OPLL and identify its three intrinsic sources of phase noises namely, randomness of received data pulses, detector's shot noise, and the FOPA noises such as amplified spontaneous emission (ASE). The ASE noise is reflected in the FOPA's noise figure parametrically. However, the effects of the other two noise sources on the proposed OPLL performance are investigated, using the power spectral densities (PSDs) of the signals involved in the OPLL. Finally, the PSDs are used to obtain a mathematical expression for the OPLL's timing jitter. From the analytical results, our proposed OPLL benefits from the FOPA's inherent large bandwidth and exhibits a very low timing jitter, which is in the order of femtosecond, for an OTDM system with 80 Gbps data rate.**

***Index Terms*—All-optical clock recovery, fiber optical parametric amplifier (FOPA), four wave mixing (FWM), highly non-linear fiber (HNLF), optical phase-lock loop (OPLL), timing jitter.**

I. Introduction

OPTICAL clock recovery (OCR) unit, which synchronizes a locally generated optical clock signal with incoming optical data, is a fundamental part of any optical communication system. In conventional optical communication systems, the clock recovery process is carried out using electronic phase-lock loop schemes, where an optical to electrical signal conversion is performed prior to the clock extraction process. However, in future ultra-high speed all-optical data communication systems with signal bandwidths above 100 GHz, the electronic circuits are considered low in speed to be used in clock recovery process. Hence, for such ultra-high speed all-optical systems, clock recovery in optical domain becomes a viable and promising solution. Recently, various schemes for all-OCR have been proposed and analyzed, ranging from self-pulsating lasers [1], [2] and filtering methods [3], [4] to PLL based solutions.

Optical phase-lock loops (OPLLs) often suffer from more setup complexity. However, the recovered clock quality is high in terms of jitter and stability, and optical PLLs provide the possibility of sub-harmonic OCR, which is essential in TDM systems.

Up until now, various types of optical PLLs are proposed, where their main difference is due to different cross-correlator schemes employed to detect the phase error between the local clock and the incoming data signal. The first optical PLL was proposed by Kawanishi and Saruwatari [5], where the cross-correlator employed a semiconductor optical amplifier (SOA) with the incoming data pulses as its input optical signal, and an RF local clock pulse stream modulating its optical gain. This PLL was further developed using optically gain modulated SOA [6]–[8]. In this type of PLLs, the output power of the SOA simulates the synchronicity of the incoming data and locally generated clock pulses.

However, instead of gain modulation, amplitude modulated optical gate can also be used to perform cross-correlation process. Several such PLLs have been proposed in [9]–[12], where a nonlinear optical loop mirror (NOLM) is used as a gating mechanism. Electronically, gated electro-absorption modulation (EAM) [13]–[20] and optically gated EAM [21]–[24] are also used for such types of PLLs. In [25], LiNbO3 modulators are used to perform gating or equivalently cross-correlation process. In [26], [27], FWM (four wave mixing) process in SOAs is proposed to perform the cross-correlation process in the OPLL. However, the SOAs have low FWM power conversion efficiency, due to their very short FWM interaction length, and also their operation is relatively bandwidth-limited.

In this paper, a new OPLL for an OTDM system, based on fiber optical parametric amplifiers (FOPA) is proposed and analyzed. The FOPAs are based on FWM process in a highly nonlinear fiber optic (HNLF), but unlike the SOAs, they can be designed for a very high power conversion efficiency [28], [29]. Furthermore, the operational bandwidth of the FOPAs can be managed to exceed hundreds of nanometers. Moreover, the center frequency of the incoming data signal can take on the whole optical communication wavelength range. FOPAs also exhibit a low noise figure (NF) that can be equivalent to those of the best optical amplifiers, and they are potentially attracting widespread interest and usage in optical communication systems. The FOPA's elegant performance in ultra-high speed optical sampling applications is investigated and confirmed in

Manuscript received April 7, 2014; revised April 27, 2014; accepted June 5, 2014. Date of publication July 10, 2014; date of current version July 19, 2014. This research was supported in part by the Iran National Science Foundation.

The authors are with the Optical Networks Research Laboratory, Electrical Engineering Department, Sharif University of Technology, Tehran, Iran (e-mail: damani@ee.sharif.edu; jasalehi@sharif.edu).

Color versions of one or more of the figures in this paper are available online at http://ieeexplore.ieee.org.

Digital Object Identifier 10.1109/JLT.2014.2329900

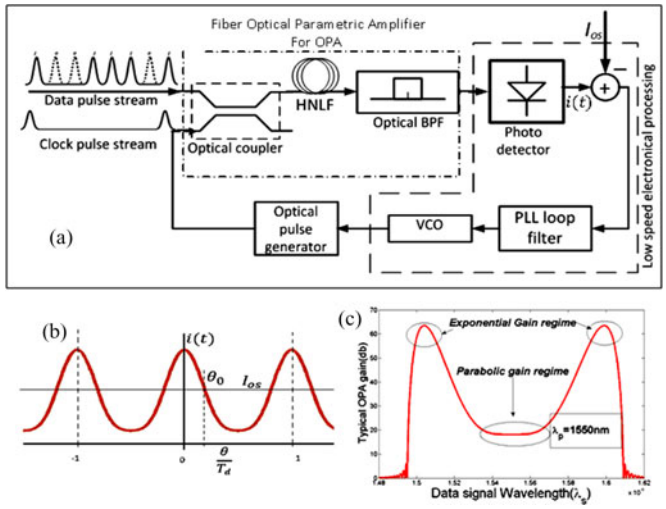

Fig. 1. (a) Proposed All-Optical PLL block diagram. (b) Photodetector's filtered output current as a function of time delay between clock and data signals, θ.(c) a typical FOPA gain spectrum.

[30]–[33]. Recently, new generations of HNLFs are introduced, encompassing holy, micro-structured and W-type optical fibers. Nonlinear coefficient of such fibers is up to four orders of magnitude greater than the nonlinear coefficient of the ordinary HNLF fibers [34], [35]. The above impressive progress in fiber nonlinearity, dramatically reduces the required excess optical power and fiber length in the FOPA. As expressed previously, this paper proposes and analyzes a new all-OCR scheme based on FOPA in optical communication systems, which can potentially be a promising clock recovery method in the future ultra-high speed optical communications.

This paper is organized as follows. In Section II, the system model and its principles of operation will be discussed. In Sections III and IV we describe the statistical model of the OPLL by analyzing its error signal and the resulted timing jitter. In Section V we investigate the analytical results obtained in the previous sections. Section VI concludes this paper. Appendices A and B exhibit the details of the analyses employed in the OPLL error signal derivation.

II. System Model and Principle of Operation

The fundamental configuration and block diagram of our proposed OPLL is shown in Fig. 1(a). As it is evident from the block diagram, the incoming data and the local clock pulses are combined via an optical coupler and injected to a highly non-linear fiber (HNLF). From the fiber optical parametric amplifier's (FOPA) theory [36], the interaction between the clock and data signals yields an amplified FWM signal known as *idler*, with an average power that is a function of the time overlapping of the clock and data pulses. The relatively high intensity clock pulse stream acts as FOPA's pump signal. The amplifier is followed by an optical band pass filter, passing through the *idler* signal only, and a low speed photo detector to detect the *idler*'s average power.

The photodetector's output current is proportional to *idler*'s average power and is used to construct the OPLL's phase error signal, which is further filtered and applied to the voltage controlled oscillator (VCO). The combination of a VCO and an optical source (where both may be compacted in one unit) generates the optical clock, which is fed back into the FOPA. With relatively short fiber length and appropriate pulse widths, the walk off effect between clock and data pulse streams can be negligible and the *idler*'s time-dependent power can be derived using quasi-continuous wave (CW) FOPA solutions [36]. Thus, in our pulsed pump FOPA, the *idler* power signal, $P_{id}(t)$, equals to

$$P_{\mathrm{id}}(t) = P_d(0,t)\left(\frac{\gamma P_c(t-\theta)}{g(t-\theta)}\right)^2 \sinh^2(g(t-\theta)L) = P_d(0,t)G(t) \tag{1}$$

where, L, γ, θ, $P_c(t)$, and $P_d(0,t)$ are respectively the HNLF fiber length, fiber nonlinear coefficient, time delay between the clock and data pulse streams, pump (here the local clock) power and the data signal power. Here the pump is assumed not to be depleted and similarly due to relatively short fiber length, fiber attenuation coefficient is also ignored. $G(t)$ and $g(t)$ denote the FOPA gain and parametric gain coefficient, respectively, and are expressed as follows:

$$G(t) = \left(\frac{\gamma P_c(t-\theta)}{g(t-\theta)}\right)^2 \sinh^2(g(t-\theta)L) \tag{2}$$

$$g(t) = \sqrt{(\gamma P_c(t))^2 - \left(\frac{\kappa(t)}{2}\right)^2} \tag{3}$$

where $\kappa(t)$ indicates the phase mismatch factor of the FOPA, and it is responsible for group velocity dispersion due to linear dispersion and nonlinear Kerr effect.

The detector's output current, $i(t)$, which makes the OPLL's error signal, is proportional to

$$i(t)\alpha\ \langle P_{id}(t)\rangle_t = \langle P_d(0,t-\theta)\left(\frac{\gamma P_c(t)}{g(t)}\right)^2 \sinh^2(g(t)L)\rangle_t \tag{4}$$

where $\langle\cdot\rangle_t$ denotes a time averaging operation, which is imposed by the low pass electron response of the photodetector. Fig. 1(b) shows a typical photocurrent signal, $i(t)$, as a function of delay time, θ. As it can be easily seen from the figure, the error current signal contains a DC offset component, denoted by I_{os}, and should be subtracted in order to achieve a bipolar error signal. The feedback mechanism is designed to force the error signal to zero by locking the clock and data pulses together with delay, θ_0, determined by the position of zero-crossing point, as shown in Fig. 1(b).

Fig. 1(c) shows a typical spectrum of an FOPA. The maximum gain is achieved when the signal wavelength (here the data signal) satisfies the phase matching condition, i.e., $\kappa(t) \approx 0$, [36]. In this case, $g(t-\theta) = \gamma P_c(t-\theta)$ and (1) simplifies to

$$P_{\mathrm{id}}(t) = P_d(0,t)\sinh^2(\gamma P_c(t-\theta)L) = G_{\mathrm{ph}}(t)P_d(0,t) \tag{5}$$

where the gain of the FOPA in (5) is subscripted by ph to show the phase matching condition. Under this condition, we call the FOPA to be operating in phase matching or maximum gain

regime, and the corresponding gain is denoted by

$$G_{\rm ph}(t) = \sin {\rm h}^2(\gamma P_c(t-\theta)L). \tag{6}$$

Furthermore, with a data signal wavelength in the vicinity of the wavelength of the clock signal, the fiber dispersion becomes negligible and $\kappa(t) \approx 2\gamma P_c(t)$. Consequently, the FOPA gain coefficient, $g(t)$, converges to zero and (1) further simplifies to

$$P_{\rm id}(t) = P_d(0,t)(\gamma P_c(t-\theta)L)^2 = G_{\rm par}(t)P_d(0,t) \tag{7}$$

where the *idler* power becomes a parabolic function of the power of pump (here the local clock) signal. Under this condition, we call the FOPA to be working in the parabolic gain regime. The corresponding gain is subscripted by, par, to diagnose the parabolic gain condition. As shown in Fig. 1(c), the parabolic gain approximately corresponds to the minimum gain of the FOPA in its gain bandwidth. For this case, the gain is expressed as

$$G_{\rm par}(t) = (\gamma P_c(t-\theta)L)^2. \tag{8}$$

In this paper we assume the pump and signal beams to be co-polarized and injected into a polarization maintaining (PM) fiber. Using a fiber with random birefringence, the same equations hold, except the effective fiber nonlinearity decreases by a factor of $8/9$, [35], [36], which is negligible and can be compensated with an increase in the pump power by a factor of $9/8$. In a very long fiber, dispersion fluctuations may not be negligible and they will affect the resulting FOPA's gain. To avoid this effect, we assume the fiber to be well designed and have relatively short length.

In Section III, we will analyze the OPLL noise behavior using FOPA in both phase matching and parabolic gain regimes.

A. Sources of Noise in FOPA Based OPLL

Several sources of phase noise contribute to OPLL's timing jitter. The VCO's phase noise; timing jitter of the incoming data pulses; and other noises due to electronic devices are some examples. However, in this paper we do not consider any of the aforementioned noise sources, since they have identical behavior in all previously introduced PLLs and extensively studied in literature [37]–[39]. Thus, as in [40] we consider only those sources of noise that are intrinsic to our OPLL and cannot be reduced using lower noise electronic devices. In this context, three such sources of noise are of interest. The first is due to the random nature of the incoming data pulse train, whose interaction with the clock pulses produces the phase error signal, leading to some random fluctuations in the resulting error signal. The second source of noise is the shot noise due to the receiver's photodetector and the third source of noise arises from the optical amplifier, such as amplified spontaneous emission noise, noisy pump signal, and Raman gain noise [41]–[43], which, together cause an increase in NF of FOPA amplifier.

However, in this paper, for the sake of mathematical simplicity, we do not consider directly the amplifier's noises in our derivations. Instead, the effect of such noises will be reflected in the NF of the FOPA. In other words, the OSNR deterioration due to amplifier's noise will be considered by increasing the noise power resulted from the other noise sources, i.e., the data randomness and the photodetector's shot noises, by a factor of NF.

III. Statistical Modeling

To model the aforementioned noise sources, in the context of statistics, we begin by assuming that the output photocurrent from the detector, $i(t)$, is a *filtered shot noise process* [40] with $a(t)$ acting as its non-filtered equivalent. Hence, $a(t)$ is, in turn, generated by the input photon count rate process, denoted by $n(t)$, which can be expressed as

$$n(t) = \alpha P_{\rm id}(t) \tag{9}$$

where $P_{\rm id}(t)$ is the power of the *idler* signal and α is a proportionality factor and is related closely to the photodetector's quantum efficiency factor (η), Plank's constant (h) and the light frequency (f) as $\alpha = \frac{\eta}{hf}$.

Actually, the detector's photocurrent, i.e., $i(t)$, can be interpreted as $a(t)$ after passing through a filter, which is the detector's electron response, $h_e(t)$; in other words $i(t) = a(t) * h_e(t)$ where $(*)$ denotes the convolution operation. The Fourier transform of $h_e(t)$, $H_e(f)$, is such that $H_e(0) = q$, where q represents the elementary charge. Also the aforementioned offset DC current, $I_{\rm os}$, is related to DC component of $a(t)$, denoted by $A_{\rm os}$, so that the relation $A_{\rm os} = I_{\rm os}/H_e(0) = I_{\rm os}/q$ holds. Consequently subtracting $A_{\rm os}$ from $a(t)$ is equivalent to canceling the DC component of $i(t)$.

The photodetector can be modeled as a new photodetector with infinite bandwidth with output, $a(t)$, followed by a low pass filter with transform function, $H_e(f)$, which is combined with the OPLL loop filter. Hence, instead of $i(t)$, $a(t)$ can be interpreted as the OPLL's error signal. Furthermore, the mean and power spectra of $a(t)$ and $n(t)$ are closely related namely [44]

$$\overline{a(t)} = \bar{g}\overline{n(t)} \tag{10}$$

$$S_a(f) = \overline{g^2}\ \overline{n(t)} + \bar{g}^2 S_n(f) \tag{11}$$

where $S_a(f)$ and $S_n(f)$ are the power spectral densities (PSD) of $a(t)$ and $n(t)$, respectively. And $\bar{g}$ and $\overline{g^2}$ represent the first and second moments of the detector's avalanche gain.

With the above assumptions, the statistical analysis of the OPLL simplifies, specially, in obtaining the statistical properties of $n(t)$; which, in turn, requires the data and clock signal forms. In this paper we assume the clock and data signals to be of the form

$$C(t) = \sum_{m=-\infty}^{\infty} P_c(t - mT_c) \tag{12}$$

$$D(t) = \sum_{m=-\infty}^{\infty} b_m P_d(t - mT_d) \tag{13}$$

where $b_m \varepsilon \{0,1\}$represent the binary data stream in an ON-OFF keying modulation system. T_d and T_c are data and clock pulse periods in an OTDM system with N users, and are related as $T_c = NT_d$. In (12) and (13), $P_c(t)$ and $P_d(t)$ represent

zero-centered pulses of clock and data, respectively, and are assumed to be Gaussian pulses as in [40]

$$P_c(t) = \frac{\bar{P}_c\sqrt{\frac{1}{\pi}}T_c}{W}\exp\left(-\frac{t^2}{W^2}\right)\prod_{T_c}(t)$$
$$= a_c\exp\left(-\frac{t^2}{W^2}\right)\prod_{T_c}(t) \quad (14)$$

$$P_d(t) = \frac{2\bar{P}_d\sqrt{\frac{1}{\pi}}T_d}{W}\exp\left(-\frac{t^2}{W^2}\right)\prod_{T_d}(t)$$
$$= a_d\exp\left(-\frac{t^2}{W^2}\right)\prod_{T_d}(t) \quad (15)$$

where $\overline{P_c}$and $\overline{P_d}$denote the average power of clock and data signals, $\Pi_T(t)$ is a rectangular zero-centered pulse with unit height and duration, $T, T\varepsilon\{T_c, T_d\}$. The parameter, W, is the pulse width parameter and it is assumed to be the same for both clock and data pulses. The parameters a_c and a_d are defined to simplify the corresponding expressions and the factor 2 in (15) is due to the fact that the data stream consists of equally likely zeros and ones. Using the above signal forms, the count rate $n(t)$ and the θ-dependent mean value of $a(t)$ is derived, using the FOPA in both prescribed gain regimes.

A. FOPA in Phase Matching (Maximum) Gain Regime

As described in the previous section and from (10) and (11), it is necessary to obtain the statistics of $n(t)$ in order to achieve the statistics of the error signal, $a(t)$. In this subsection, the mean value of $a(t)$ is obtained assuming FOPA to be operating in phase-matching condition. From (5), (9), (12)–(15), it is easily shown that

$$n(t) = \alpha P_{\rm id}(t) = \alpha D(t)\sinh^2(\gamma LC(t-\theta)). \quad (16)$$

It can be observed that $n(t)$ is a cyclostationary random process [40]. As a result, assigning a common random phase with uniform distribution between 0 and T_c to the clock and data signals (which doesn't affect their relative time delay), makes $n(t)$ a stationary random process with time independent statistics. Assuming the clock and data pulse widths not to be significantly different, it will be reasonable to assume each clock pulse to be restricted in the time duration of two consecutive data pulses in the OTDMA system, as illustrated in Fig. 2. So, the time-independent mean value of $a(t)$, conditioned on a fixed time difference $\theta\in[0,T_d]$, can be expressed as (A11)

$$\bar{a} = \bar{g}\overline{n(t)} = \bar{g}\frac{\alpha W^2\pi a_d}{2T_c^2\sqrt{2}}\sum_{l=1}^{\infty}\frac{(2\gamma La_c)^{2l}}{(2l)!\sqrt{l}}$$
$$\times\left\{1+2\sum_{k=1}^{\infty}\exp\left(-\frac{k^2\omega_c^2W^2}{4}\left(1+\frac{1}{2l}\right)\right)\right.$$
$$\left.\times\cos\left(\frac{k\omega_cT_d}{2}\right)\cos\left(k\omega_c\left(\theta-\frac{T_d}{2}\right)\right)\right\} \quad (17)$$

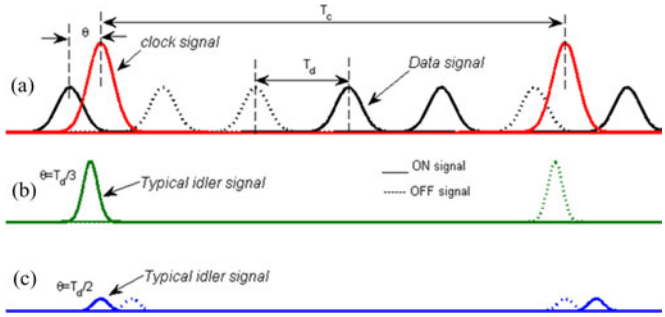

Fig. 2. (a) Typical signals of an OTDM system. (b) and (c) Resulting *idler* signals with different delay times, θ.

where $\omega_c = \frac{2\pi}{T_c}$ is the angular frequency of the clock pulse rate.

B. FOPA in Parabolic Gain Regime

Using the FOPA in its parabolic gain regime, we repeat the process of the previous subsection. From (7), (9), (12)–(15); $n(t)$ can be expressed as

$$n(t) = \alpha P_{\rm id}(t) = \alpha D(t)(\gamma LC(t-\theta))^2 = \alpha a_d(\gamma La_c)^2$$
$$\times\sum_{m=-\infty}^{\infty}\sum_{n=-\infty}^{\infty}b_m e^{-\frac{(t-mT_d)^2}{W^2}}e^{-\frac{2(t-nT_c-\theta)^2}{W^2}}\prod_{T_d}$$
$$\times(t-mT_d)\prod_{T_c}(t-nT_c-\theta). \quad (18)$$

With the conditions described previously, the θ-dependent mean value of $a(t)$ can be derived as (A12)

$$\bar{a} = \bar{g}\overline{n(t)} = \bar{g}\frac{\alpha W^2\pi a_d(\gamma La_c)^2}{T_c^2\sqrt{2}}$$
$$\times\left\{1+2\sum_{k=1}^{\infty}\exp\left(-\frac{3k^2\omega_c^2W^2}{8}\right)\cos\left(\frac{k\omega_cT_d}{2}\right)\right.$$
$$\left.\times\cos\left(k\omega_c\left(\theta-\frac{T_d}{2}\right)\right)\right\}. \quad (19)$$

The parameter $\bar{a}$, derived in the above, is time-independent and resembles the low-speed photodetector's output current as a function of time delay θ. The elements of the series in (17) and (19) converge rapidly to zero, and practically only the first few elements are needed to be considered.

IV. OPLL Error Signal Analysis

In this section, the OPLL's error signal, $a(t)$, will be analyzed in order to obtain a closed form expression for the OPLL's output timing jitter. As previously mentioned, the θ-dependent mean, $\bar{a}$, resembles the output current of the photo detector and its DC offset should be cancelled in order to obtain a bipolar error signal. However, the signal, $a(t)$, has random fluctuations due to prescribed noises, and it can be written as the sum of its mean, $\bar{a}$, and a zero-mean additive noise $\nu(t)$. As in [40], we linearly approximate the error signal, $a(t)-A_{\rm os}$, in the vicinity of the

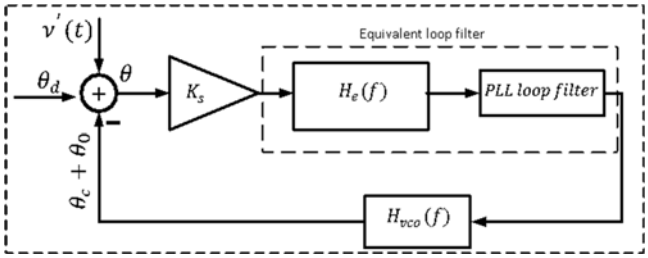

Fig. 3. OPLL's phase-domain model.

operating point, θ_0. So we can express the error signal as

$$a(t) - A_{os} = (\bar{a} - A_{os}) + \nu(t) = K_s(\theta - \theta_0) + \nu(t)$$
$$= K_s(\theta + \nu'(t) - \theta_0) \tag{20}$$

where $\nu'(t) = \frac{\nu(t)}{K_s}$ is an equivalent noise term and K_s is the slope of $\bar{a}$ at $\theta = \theta_0$and can be derived by evaluating the derivative of (17) and (19) with respect to θ; hence,

A. With FOPA in Phase Matching Gain Regime

$$K_s = -\frac{\bar{g}\alpha W^2 \pi a_d}{T_c^2\sqrt{2}} \sum_{l=1}^{\infty} \frac{(2\gamma L a_c)^{2l}}{(2l)!\sqrt{l}} \times \left\{ \sum_{k=1}^{\infty} k\omega_c \exp\left(-\frac{k^2\omega_c^2 W^2}{4}\left(1+\frac{1}{2l}\right)\right) \cos\left(\frac{k\omega_c T_d}{2}\right) \times \sin\left(k\omega_c\left(\theta_0 - \frac{T_d}{2}\right)\right)\right\}. \tag{21}$$

B. With FOPA in Parabolic Gain Regime

$$K_s = -\bar{g}\frac{2\alpha W^2 \pi a_d (\gamma L a_c)^2}{T_c^2\sqrt{2}} \times \left\{ \sum_{k=1}^{\infty} k\omega_c \exp\left(-\frac{3k^2\omega_c^2 W^2}{8}\right) \cos\left(\frac{k\omega_c T_d}{2}\right) \times \sin\left(k\omega_c\left(\theta_0 - \frac{T_d}{2}\right)\right)\right\}. \tag{22}$$

Fig. 3 illustrates the linear model of the OPLL in phase domain. In this linear model, the relative time delay, θ, is expressed as the difference of the absolute phases of data and clock signals, i.e., $\theta = \theta_d - \theta_c$, where θ_d and θ_c denote the phases of data and clock signals, respectively. As it is evident from the figure, the term $\nu'(t)$ shows the OPLL's equivalent noise at the system input; and (20) becomes of the form

$$a(t) - A_{os} = K_s(\theta_d + \nu'(t) - (\theta_c + \theta_0)). \tag{23}$$

From the OPLL's phase domain representation, it is obvious that the timing jitter of the OPLL can be interpreted as the system's response to the input noise, $\nu'(t)$. Thus, it's variance is related to the PSD of $\nu'(t)$, $S'_\nu(f)$, as

$$\sigma_p^2 = \mathrm{NF}\int_{-\infty}^{\infty} S_{\nu'}(f)\,|G(f)|^2\,df = \mathrm{NF}\int_{-\infty}^{\infty}\frac{S_\nu(f)}{K_s^2}\,|G(f)|^2\,df$$
$$= \mathrm{NF}\frac{S_\nu(0)}{K_s^2}\int_{-\infty}^{\infty}|G(f)|^2\,df = \frac{2S_\nu(0)}{K_s^2}\mathrm{NFB}_f \tag{24}$$

where, in writing (24), we assume the closed-loop bandwidth of the OPLL to be much narrower compared to the broadband PSD of $\nu'(t)$, which is considered to be a practical assumption; *NF* is the FOPA's NF; $G(f)$ and B_f denote the closed-loop frequency response, and equivalent (one sided) bandwidth of the OPLL, and can be expressed as

$$G(f) = \frac{K_s H_e(f) H_{\mathrm{PLL}}(f) H_{\mathrm{VCO}}(f)}{1 + K_s H_e(f) H_{\mathrm{PLL}}(f) H_{\mathrm{VCO}}(f)} \tag{25}$$

$$B_f = \int_0^{\infty} |G(f)|^2\,df. \tag{26}$$

As indicated in (24), we should obtain $S_\nu(0)$, i.e., the PSD of $\nu(t)$ at DC frequency, in order to obtain the value of σ_p^2. But from (20), it is easily shown that:

$$S_\nu(0) = S_a(f)\mid_{f=0} - \bar{a}^2\delta(f). \tag{27}$$

And from (11), $S_a(f)\mid_{f=0} = \overline{g^2}\bar{n} + \bar{g}^2 S_n(f)\mid_{f=0}$. Where $\bar{n}$ is obtained in (A10) and (A11) and the PSD of $n(t)$ can be derived for the two cases of FOPA gain regimes as following [see Appendix B].

C. FOPA in Phase Matching Gain Regime

Using FOPA in phase matching condition, the PSD of $n(t)$ at DC frequency is derived in (B22), and multiplying the result by $\bar{g}^2$ yields

$$\bar{g}^2 S_n(f)|_{f=0} = \bar{g}^2\frac{(\alpha W^2 a_d \pi)^2}{32T_C^3}\left\{\left(\sum_{l=1}^{\infty}\frac{(2\gamma L a_C)^{2l}}{(2l)!\sqrt{l}}\left[1 + 2\sum_{k=1}^{\infty}\exp\left(-\frac{k^2\omega_C^2 W^2}{4}\left(1+\frac{1}{2l}\right)\right)\cos(k\omega_C\theta)\right]\right)^2 + \left(\sum_{l=1}^{\infty}\frac{(2\gamma L a_C)^{2l}}{(2l)!\sqrt{l}}\left[1 + 2\sum_{k=1}^{\infty}\exp\left(-\frac{k^2\omega_C^2 W^2}{4}\left(1+\frac{1}{2l}\right)\right)\cos(k\omega_C(\theta + T_d))\right]\right)^2\right\} + \bar{g}^2\bar{n}^2\delta(f). \tag{28}$$

D. FOPA in Parabolic Gain Regime

For this case, (28) becomes as

$$\begin{aligned}
&\bar{g}^2 S_n(f)|_{f=0} \\
&\quad = \frac{\bar{g}(\alpha a_d \pi)^2(\gamma L a_C W)^4}{4T_C^3}\frac{(\alpha a_d\pi)^2(\gamma L a_C W)^4}{4T_C^3} \\
&\qquad \times \left\{\left(1+2\sum_{k=1}^{\infty}\exp\left(-\frac{3k^2\omega_C^2W^2}{8}\right)\cos(k\omega_C\theta)\right)^2\right. \\
&\qquad + \left(1+2\sum_{k=1}^{\infty}\exp\left(-\frac{3k^2\omega_C^2W^2}{8}\right)\cos(k\omega_C(\theta\right. \\
&\qquad \left.\left.+T_d))\right)^2\right\} + \bar{g}^2\bar{n}^2\delta(f). \qquad (29)
\end{aligned}$$

The terms including delta functions in (28) and (29), are related closely to DC part of $a(t)$ and can be expressed as $\bar{g}^2\bar{n}^2\delta(f) = \bar{a}^2\delta(f)$. The expression for $S_a(f)\mid_{f=0}$ can be obtained by substituting (28), (29) and $\overline{n(t)}$ in (11); and substituting the result in (27) yields $S_\nu(0)$ as follows.

E. FOPA in Phase Matching Gain Regime

$$\begin{aligned}
&S_v(0) \\
&= \bar{g}^2\frac{(\alpha W^2 a_d\pi)^2}{32T_C^3}\left\{\left(\sum_{l=1}^{\infty}\frac{(2\gamma L a_C)^{2l}}{(2l)!\sqrt{l}}\left[1\right.\right.\right. \\
&\quad \left.\left.+2\sum_{k=1}^{\infty}\exp\left(-\frac{k^2\omega_C^2W^2}{4}\left(1+\frac{1}{2l}\right)\right)\cos(k\omega_C\theta)\right]\right)^2 \\
&\quad + \left(\sum_{l=1}^{\infty}\frac{(2\gamma L a_C)^{2l}}{(2l)!\sqrt{l}}\left[1+2\sum_{k=1}^{\infty}\right.\right. \\
&\quad \left.\left.\left.\exp\left(-\frac{k^2\omega_C^2W^2}{4}\left(1+\frac{1}{2l}\right)\right)\cos(k\omega_C(\theta+T_d))\right]\right)^2\right\} \\
&\quad + FA\frac{\bar{g}^2\alpha W^2\pi a_d}{2T_C^2\sqrt{2}}\sum_{l=1}^{\infty}\frac{(2\gamma L a_C)^{2l}}{(2l)!\sqrt{l}}\left\{1\right. \\
&\quad + 2\sum_{k=1}^{\infty}\exp\left(-\frac{k^2\omega_C^2W^2}{4}\left(1+\frac{1}{2l}\right)\right) \\
&\quad \left.\cos\left(\frac{k\omega_C T_d}{2}\right)\cos\left(k\omega_C\left(\theta-\frac{T_d}{2}\right)\right)\right\}. \qquad (30)
\end{aligned}$$

F. With FOPA in Parabolic Regime

$$\begin{aligned}
S_v(0) &= \bar{g}^2\frac{(\alpha a_d\pi)^2(\gamma L a_C W)^4}{4T_C^3} \\
&\quad \times\left\{\left(1+2\sum_{k=1}^{\infty}\exp\left(-\frac{3k^2\omega_C^2W^2}{8}\right)\cos(k\omega_C\theta)\right)^2\right. \\
&\quad + \left(1+2\sum_{k=1}^{\infty}\exp\left(-\frac{3k^2\omega_C^2W^2}{8}\right)\right. \\
&\quad \left.\left.\times\cos(k\omega_C(\theta+T_d))\right)^2\right\} + \mathrm{FA}\frac{\bar{g}^2\alpha W^2\pi a_d(\gamma L a_C)^2}{T_C^2\sqrt{2}} \\
&\quad \times\left\{1+2\sum_{k=1}^{\infty}\exp\left(-\frac{3k^2\omega_C^2W^2}{8}\right)\cos\left(\frac{k\omega_C T_d}{2}\right)\right. \\
&\quad \left.\times\cos\left(k\omega_C\left(\theta-\frac{T_d}{2}\right)\right)\right\} \qquad (31)
\end{aligned}$$

where $\mathrm{FA} = \frac{\overline{g^2}}{\bar{g}^2}$ is the excess noise factor of the avalanche photodiode.

The second terms in the right hand side of (30) and (31) account for shot noise, while the first terms describe the noise originated from the data sequence randomness.

Substituting (21), (26) and (30) in (24), yields the variance of the OPLL's timing jitter, using FOPA in phase matching condition, as follows:

$$\begin{aligned}
\sigma_{\mathrm{ph}}^2 &= \frac{T_c\mathrm{NFB}_f}{8}\frac{f_1(\theta_0)+f_1(\theta_0+T_d)}{f_2(\theta_0)} \\
&\quad + \frac{\sqrt{2}\mathrm{NF}.B_f.\mathrm{FA}.T_c^2}{\pi\alpha W^2 a_d}\frac{f_3(\theta_0)}{f_2(\theta_0)} \\
&= \mathrm{NF}(\sigma_{\mathrm{ph-bin}}^2+\sigma_{\mathrm{ph-shot}}^2). \qquad (32)
\end{aligned}$$

Also, the variance of the OPLL's timing jitter using FOPA in parabolic gain regime can be obtained, substituting (22), (26) and (31) in (24) as follows:

$$\begin{aligned}
\sigma_{\mathrm{par}}^2 &= \frac{\mathrm{NFB}_f T_c}{4}\frac{f_4(\theta_0)+f_4(\theta_0+T_d)}{f_5(\theta_0)} \\
&\quad + \frac{\sqrt{2}\mathrm{NF}.B_f.\mathrm{FA}.T_c^2}{2\pi a_d\alpha(W\gamma L a_c)^2}\frac{f_6(\theta_0)}{f_5(\theta_0)} \\
&= \mathrm{NF}(\sigma_{\mathrm{par-bin}}^2+\sigma_{\mathrm{par-shot}}^2) \qquad (33)
\end{aligned}$$

where

$$\begin{aligned}
f_1(\theta) &\underline{\underline{\mathrm{def}}}\left(\sum_{l=1}^{\infty}\frac{(2\gamma L a_c)^{2l}}{(2l)!\sqrt{l}}\left[1+2\sum_{k=1}^{\infty}\exp\right.\right. \\
&\quad \left.\left.\left(-\frac{k^2\omega_c^2W^2}{4}\left(1+\frac{1}{2l}\right)\right)\cos(k\omega_c\theta)\right]\right)^2 \qquad (34)
\end{aligned}$$

$$\begin{aligned}
f_2(\theta) &\underline{\underline{\mathrm{def}}}\left(\sum_{l=1}^{\infty}\frac{(2\gamma L a_c)^{2l}}{(2l)!\sqrt{l}}\left\{\sum_{k=1}^{\infty}k\omega_c\exp\right.\right. \\
&\quad \left(-\frac{k^2\omega_c^2W^2}{4}\left(1+\frac{1}{2l}\right)\right)\cos\left(\frac{k\omega_c T_d}{2}\right) \\
&\quad \left.\left.\sin\left(k\omega_c\left(\theta-\frac{T_d}{2}\right)\right)\right\}\right)^2 \qquad (35)
\end{aligned}$$

$$f_3(\theta) \underline{\underline{\text{def}}} \sum_{l=1}^{\infty} \frac{(2\gamma L a_c)^{2l}}{(2l)!\sqrt{l}} \left\{ 1 + 2\sum_{k=1}^{\infty} \exp\left(-\frac{k^2\omega_c^2 W^2}{4}\left(1+\frac{1}{2l}\right)\right) \cos\left(\frac{k\omega_c T_d}{2}\right) \cos\left(k\omega_c\left(\theta - \frac{T_d}{2}\right)\right)\right\} \quad (36)$$

$$f_4(\theta) \underline{\underline{\text{def}}} \left(1 + 2\sum_{k=1}^{\infty} \exp\left(-\frac{3k^2\omega_c^2 W^2}{8}\right)\cos(k\omega_c\theta)\right)^2 \quad (37)$$

$$f_5(\theta) \underline{\underline{\text{def}}} \left\{ \sum_{k=1}^{\infty} k\omega_c \exp\left(-\frac{3k^2\omega_c^2 W^2}{8}\right)\cos\left(\frac{k\omega_c T_d}{2}\right) \sin\left(k\omega_c\left(\theta_0 - \frac{T_d}{2}\right)\right)\right\}^2 \quad (38)$$

$$f_6(\theta) \underline{\underline{\text{def}}} \left\{ 1 + 2\sum_{k=1}^{\infty} \exp\left(-\frac{3k^2\omega_c^2 W^2}{8}\right)\cos\left(\frac{k\omega_c T_d}{2}\right) \cos\left(k\omega_c\left(\theta - \frac{T_d}{2}\right)\right)\right\}. \quad (39)$$

The subscripts par and ph in (32) and (33) denote the parabolic and phase-matching gain regimes of the FOPA; while subscripts *shot* and *bin* indicate the origin of the corresponding variance terms, i.e., shot noise and noise due to random binary data, respectively.

V. Numerical Results and Discussions

In this section, we investigate the analytical results obtained in the previous section. To do so, we set $\bar{P}_d = 6$ mW, $\bar{P}_c = 12$ mW (which corresponds to average powers of 3 and 6 mWatt, in passband, for data and clock signals, respectively). Also as reported in [40], we choose $T_d = 12.5$ ps, $T_c = 100$ ps, pulsewidth of data and clock signals (FWHM) $= 4$ ps, $B_f = 5.5$ kHz, $\bar{g} = 150$, FA $= 5$ and $\theta_0 = T_d/4$.

In addition, for the FOPA, we choose the fiber length $L = 50$ m (L considered to be short enough to avoid the walk off effect); fiber nonlinear coefficient $(\gamma) = 0.02\ (\mathrm{W}\cdot\mathrm{m})^{-1}$); fiber zero-dispersion wavelength $(\lambda_{zdw}) = 1.550\ \mu$m; data signal wavelength (for phase-matching condition) $= 1.50\ \mu$m; and detector's quantum efficiency factor $(\eta) = 50$ (i.e., $\alpha = 4 \times 10^{18}$). Also, the wavelength of the local clock signal is set to the zero-dispersion wavelength of the fiber (λ_{zdw}), i.e., second order dispersion parameter, $\beta_2 = 0$, and third and forth order dispersion parameters are chosen as $\beta_3 = 1.2 \times 10^{-40}\ \mathrm{S}^3/\mathrm{m}$, $\beta_4 = -5 \times 10^{-55}\ \mathrm{S}^4/\mathrm{m}$. Fig. 4(a) shows the timing jitter of our proposed OPLL and the TPA-based OPLL analyzed in [40], as a function of delay time, θ. As shown in the figure, our proposed OPLL has a timing jitter about 2 fs, which is about ten times smaller than the timing jitter of the TPA-based OPLL. We can relate this performance improvement to the higher power conversion efficiency in the FOPA (due to its long FWM interaction length) in comparison with the TPA process. Also the FOPA's potential to exhibit an exponential response is another advantage that makes it different from the TPA with quadratic response.

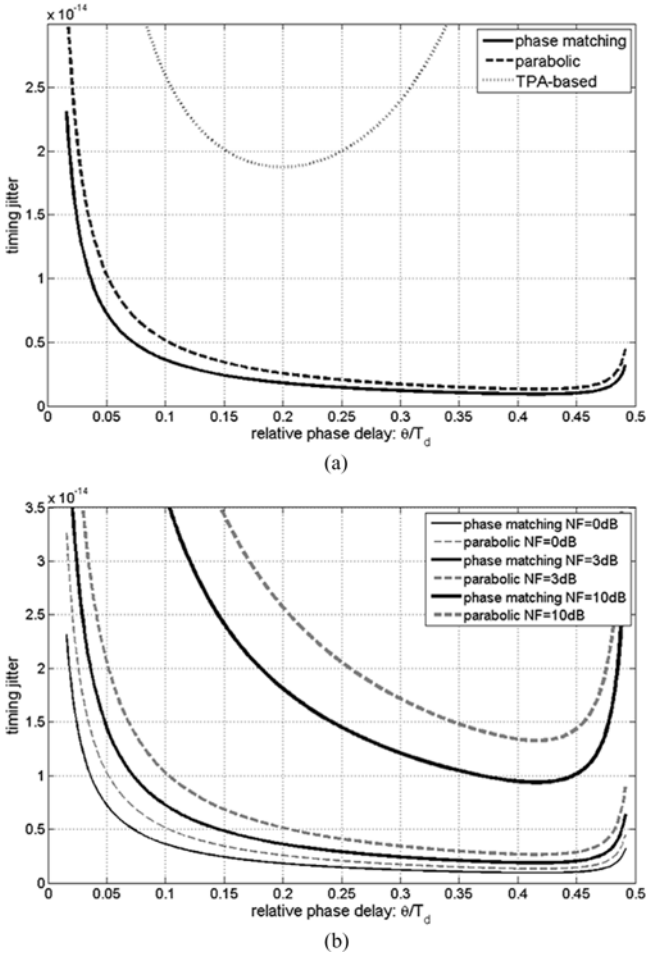

Fig. 4. (a) Comparing timing jitter of our proposed OPLL based on FOPA with NF $= 1$ and TPA-based OPLL presented in [40]. (b) The NF effect on our proposed OPLL.

The FOPA's noise behavior, thoroughly investigated in [42], [43], [45], indicates that the phase-insensitive FOPA's NF is quantum limited to 3dB and grows with other noise sources, such as the FOPA's pump noise. Fig. 4(b) shows the effect of *NF* on timing jitter. As it is shown, even a strong NF of 10 dB leads to a timing jitter to about 20 fs. The Figure also shows that, the OPLL has slightly better performance, if using FOPA in phase-matching condition rather than the parabolic gain regime. But as stated in [42], [43], [45], the FOPA is expected to have a smaller NF with parabolic gain, and this phenomenon may compensate the slightly lower performance of the corresponding OPLL.

Practically, the noises from other electronic devices will dominate and the above noises may be negligible.

VI. Conclusion

Though the FOPAs have been studied and investigated for many applications such as optical amplifiers, wavelength conversion, optical sampling, etc., the results of this paper show

their excellent capabilities to be used in super fast all-OCR applications with excellent performance achievement. The FOPAs are based on instantaneous Kerr effect, which makes them a promising solution for ultrafast optical communication clock recovery. The approximately same results obtained for both conditions of parabolic and phase-matching gain, ensure us that the FOPA as illustrated in Fig. 1(c) can be used in its entire bandwidth for clock recovery applications, and this indicates the robustness of the FOPA for OPLL applications. The potential of newly introduced HNLF fibers with very high nonlinear coefficients, which reduces the required optical powers and fiber length, enhances the FOPA's capabilities in all-optical processing applications such as OPLL in ultra-high speed optical communication systems. A reduced fiber length decreases the dispersion effect and consequently, shorter pulses can be used in FOPAs. Dispersion compensation is another technique that can be studied to overcome the pulse width limitations.

APPENDIX A

In this Appendix, the mean value of $n(t)$, i.e., $\bar{n}$, is derived, using FOPA's both, phase-matching and parabolic, gain regimes. In the remainder, we denote $n(t)$ by $n_{\rm ph}(t)$ and $n_{\rm par}(t)$ for FOPA's phase-matching and parabolic gain regimes, respectively. Using (16) and (21), we have

$$n_{\rm ph}(t) = \alpha P_{\rm id}(t) = \alpha D(t) \sin {\rm h}^2(\gamma LC(t-\theta)) \quad \text{(A1)}$$

$$n_{\rm par}(t) = \alpha P_{\rm id}(t) = \alpha D(t)(\gamma LC(t-\theta))^2. \quad \text{(A2)}$$

The expressions $\sinh^2(\gamma LC(t-\theta))$ and $(\gamma LC(t-\theta))^2$ in (A1) and (A2) are functions of the local clock signal, $C(t)$, and are periodic with period T_c. Thus, they can be represented in Fourier series as follows:

$$\sin {\rm h}^2(\gamma LC(t-\theta)) = \sum_{k=-\infty}^{\infty} A_k e^{-jk\omega_c t} \triangleq C_{\rm ph}(t) \quad \text{(A3)}$$

$$(\gamma LC(t-\theta))^2 = \sum_{k=-\infty}^{\infty} B_k e^{-jk\omega_c t} \triangleq C_{\rm par}(t) \quad \text{(A4)}$$

$$A_k = \frac{W}{2Tc}\sqrt{\frac{\pi}{2}} \sum_{l=1}^{\infty} \frac{(2\gamma La_c)^{2l}}{(2l)!\sqrt{l}} \exp\left(-\frac{k^2\omega_c^2 W^2}{8l} + jk\omega_c\theta\right) \quad \text{(A5)}$$

$$B_k = \frac{W(\gamma La_c)^2}{Tc}\sqrt{\frac{\pi}{2}} \exp\left(-\frac{k^2\omega_c^2 W^2}{8} + jk\omega_c\theta\right) \quad \text{(A6)}$$

$$\omega_c = \frac{2\pi}{T_c}. \quad \text{(A7)}$$

In deriving (A5), the complicated exponential terms of $\sin h^2(\gamma LC(t-\theta))$ are expanded in tailor series prior to performing the corresponding Fourier integration.

Assuming each clock pulse to overlap with only two consecutive data pulses; (A1) and (A2) can be rewritten as

$$n_{\rm ph}(t) = \alpha a_d \left(\sum_m b_{mN} e^{-\frac{(t-mT_c)^2}{W^2}} \prod_{T_d}(t-mT_c) + \sum_m b_{mN+1} e^{-\frac{(t-mT_c-T_d)^2}{W^2}} \prod_{T_d}(t-mT_c-T_d) \right) \times C_{ph}(t) \quad \text{(A8)}$$

$$n_{\rm par}(t) = \alpha a_d \left(\sum_m b_{mN} e^{-\frac{(t-mT_c)^2}{W^2}} \prod_{T_d}(t-mT_c) + \sum_m b_{mN+1} e^{\frac{-(t-mT_c-T_d)^2}{W^2}} \prod_{T_d}(t-mT_c-T_d) \right) \times C_{\rm par}(t). \quad \text{(A9)}$$

In writing (A8) and (A9), we have used the relation $T_c = NT_d$, and in our N user TDM system, the clock recovery for the user with data pulse stream indexed by, $(m = \cdots -N, 0, N, 2N, \ldots)$, is of interest.

As described previously, a common random phase with uniform distribution over$(0, T_c)$, denoted by t', will be considered for both data and clock signals in order to obtain time independent statistics for $n_{\rm ph}(t)$ and $n_{\rm par}(t)$. Ensemble averaging (A8) and (A9), over random data bit sequences and the prescribed common random phase, yield the following expression:

$$\begin{aligned}\bar{n}_i &= \frac{1}{T_C}\int_0^{T_C} E\left\{n_i(t-t')|t'\right\} dt' \\ &= \frac{\alpha}{2T_C} a_d \left(\sum_{m=-\infty}^{+\infty} \int_{t-(m+1)T_C}^{t-mTc} e^{-\frac{t_1^2}{W^2}} C_i(t_1)\Pi_{T_d}(t_1)dt_1 \right. \\ &\quad \left. + \sum_m \int_{t-(m+1)T_C}^{t-mT_C} e^{-\frac{(t_1-T_d)^2}{W^2}} C_i(t_1)\Pi_{T_d}(t_1-T_d)dt_1 \right) \\ &\quad \frac{\alpha}{2T_C} a_d \left\{ \int_{-\infty}^{\infty} e^{-\frac{t_1^2}{W^2}} C_i(t_1) + \int_{-\infty}^{\infty} e^{-\frac{(t_1-T_d)^2}{W^2}} C_i(t_1)dt_1 \right\}\end{aligned} \quad \text{(A10)}$$

where the index $i = {\rm par}, {\rm ph}$, and for the integrals in the second equality, a variable conversion from $t - t' - mT_c$ to t_1 was applied. Also, the Gaussian data pulses are assumed to have a high extinction ratio, which allows us to ignore the square pulses, $\prod_{T_d}(.)$.

Substituting (A3) and (A4) into (A10) and performing the integrations; (A10) yields the following expressions for the mean value of $n(t)$

$$\bar{n}_{\rm ph} = \frac{\alpha W^2 \pi a_d}{2T_c^2\sqrt{2}} \sum_{l=1}^{\infty} \frac{(2\gamma La_c)^{2l}}{(2l)!\sqrt{l}} \left\{ 1 + 2\sum_{k=1}^{\infty} \exp\left(-\frac{k^2\omega_c^2 W^2}{4}\left(1+\frac{1}{2l}\right)\right) \cos\left(\frac{k\omega_c T_d}{2}\right) \cos\left(k\omega_c\theta - \frac{k\omega_c T_d}{2}\right) \right\} \quad \text{(A11)}$$

$$\bar{n}_{\rm par} = \frac{\alpha W^2 \pi a_d (\gamma L a_c)^2}{T_c^2 \sqrt{2}} \left\{ 1 + 2 \sum_{k=1}^{\infty} \exp\left(-\frac{3k^2 \omega_c^2 W^2}{8} \right) \cos\left(\frac{k\omega_c T_d}{2} \right) \cos\left(k\omega_c \left(\theta - \frac{T_d}{2} \right) \right) \right\}. \quad \text{(A12)}$$

APPENDIX B

In this appendix, the autocorrelation function of $n(t)$, i.e., $R_n(\tau)$, and its Fourier transform at DC frequency, i.e., $S_n(0)$, will be obtained.

Using the assumptions made in Appendix A, the autocorrelation function is given by

$$\begin{aligned} R_n(\tau) &= E\left\{ n(t-t') n(t-t'-\tau) \right\} \\ &= \frac{1}{T_c} \int_0^{T_c} E\left\{ n(t-t') n(t-t'-\tau) | t' \right\} dt' \\ &= \frac{1}{T_c} \int_{t-T_c}^{t} E\{ n(t_1) n(t_1-\tau) | t_1 \} dt_1 \\ &= \frac{1}{T_c} \int_0^{T_c} E\{ n(t_1) n(t_1-\tau) | t_1 \} dt_1 \end{aligned} \quad \text{(B1)}$$

where $t_1 = t - t'$ and has the same pdf as $t\prime$.

The last equality in (B1) arises from the fact, that $E\{n(t_1)n(t_1-\tau)|t_1\}$ is a periodic function of t_1 with period, T_c; thus, its integration over one period is independent of the period, in which the integration is carried out.

Using (A8) and (A9), the integrand of (B1) is expanded as

$$\begin{aligned} n_i(t) n_i(t-\tau) = N_1(t,\tau) + N_2(t,\tau) \\ + N_3(t,\tau) + N_4(t,\tau) \end{aligned} \quad \text{(B2)}$$

where

$$\begin{aligned} N_1(t,\tau) = \alpha^2 a_d^2 \sum_n \sum_m b_{mN} b_{nN} e^{-\frac{(t-mT_c)^2}{W^2}} e^{-\frac{(t-nT_c-\tau)^2}{W^2}} \\ \times C_i(t) C_i(t-\tau) \prod_{T_d} (t - mT_c) \prod_{T_d} \\ \times (t - nT_c - \tau) \end{aligned} \quad \text{(B3)}$$

$$\begin{aligned} N_2(t,\tau) = \alpha^2 a_d^2 \sum_n \sum_m b_{mN} b_{nN+1} e^{-\frac{(t-mT_c)^2}{W^2}} e^{-\frac{(t-nT_c-\tau-T_d)^2}{W^2}} \\ \times C_i(t) C_i(t-\tau) \prod_{T_d} (t - mT_c) \prod_{T_d} \\ \times (t - nT_c - \tau - T_d) \end{aligned} \quad \text{(B4)}$$

$$\begin{aligned} N_3(t,\tau) = \alpha^2 a_d^2 C_i(t) C_i(t-\tau) \\ \times \sum_n \sum_m b_{mN+1} b_{nN} e^{-\frac{(t-mT_c-T_d)^2}{W^2}} e^{-\frac{(t-nT_c-\tau)^2}{W^2}} \prod_{T_d} \\ \times (t - mT_c - T_d) \prod_{T_d} (t - nT_c - \tau) \end{aligned} \quad \text{(B5)}$$

$$\begin{aligned} N_4(t,\tau) = \alpha^2 a_d^2 C_i(t) C_i(t-\tau) \\ \times \sum_n \sum_m b_{mN+1} b_{nN+1} e^{-\frac{(t-mT_c-T_d)^2}{W^2}} e^{-\frac{(t-nT_c-T_d-\tau)^2}{W^2}} \\ \times \prod_{T_d} (t - mT_c - T_d) \prod_{T_d} (t - nT_c - T_d - \tau) \end{aligned} \quad \text{(B6)}$$

where $i = \text{ph}, \text{par}$.

Substituting (B2)–(B6) in (B1); the autocorrelation simplifies to

$$\begin{aligned} R_n(\tau) = \frac{1}{T_c} \int_0^{Tc} E\{ N_1(t_1,\tau) | t_1 \} dt_1 \\ + \frac{1}{T_c} \int_0^{Tc} E\{ N_2(t_1,\tau) | t_1 \} dt_1 \\ + \frac{1}{T_c} \int_0^{Tc} E\{ N_3(t_1,\tau) | t_1 \} dt_1 \\ + \frac{1}{T_c} \int_0^{Tc} E\{ N_4(t_1,\tau) | t_1 \} dt_1. \end{aligned} \quad \text{(B7)}$$

Assuming the Gaussian pulses to have sufficiently high extinction ratio, the first integration in (B7) becomes

$$\begin{aligned} I_1 = \int_0^{T_C} E\left\{ N_1(t_1,\tau) | t_1 \right\} dt_1 \\ = \frac{\alpha \eta^2 a_d^2}{2} \int_0^{T_C} \sum_m e^{-\frac{(t-mT_C)^2}{W^2}} e^{-\frac{(t-mT_C-\tau)^2}{W^2}} \\ \times C_i(t) C_i(t-\tau) dt_1 + \frac{\alpha^2 a_d^2}{4} \int_0^{T_C} \sum_m \sum_{n \neq m} \\ \times e^{-\frac{(t-mT_C)^2}{W^2}} e^{-\frac{(t-nT_C-\tau)^2}{W^2}} C_i(t) C_i(t-\tau) dt_1. \end{aligned} \quad \text{(B8)}$$

Changing the order of summation and integration operators and applying appropriate variable conversion, (B8) becomes

$$\begin{aligned} I_1 = \frac{\alpha^2 a_d^2}{2} \sum_m \int_{-mT_C}^{-mT_C+T_C} e^{-\frac{(t-mT_C)^2}{W^2}} e^{-\frac{(t-mT_C-\tau)^2}{W^2}} \\ \times C_i(t) C_i(t-\tau) dt + \frac{\alpha^2 a_d^2}{4} \sum_m \int_{-mT_C}^{-mT_C+T_C} \\ \times \sum_{k \neq 0} e^{-\frac{(e-mT_C)^2}{W^2}} e^{-\frac{(t-kT_C-\tau)^2}{W^2}} C_i(t) C_i(t-\tau) dt \\ = \frac{\alpha^2 a_d^2}{4} \int_{-\infty}^{\infty} e^{-\frac{t^2}{W^2}} C_i(t) e^{-\frac{(t-\tau)^2}{W^2}} C_i(t-\tau) dt. \end{aligned} \quad \text{(B9)}$$

In order to achieve the last equality in (B9), the term with respect to $k = 0$ is added and subtracted from the equation. Also we have used the fact that the function $C_i(t)$ is periodic with period, T_c. Using convolution operator, (B9) simplifies to

$$\begin{aligned} I_1 = \frac{\alpha^2 a_d^2}{4} \left\{ e^{-\frac{t^2}{W^2}} C_i(t) \right\} * \left\{ e^{-\frac{t^2}{W^2}} C_i(-t) \right\} + \frac{\alpha^2 a_d^2}{4} \\ \times \left\{ e^{-\frac{t^2}{W^2}} C_i(t) \right\} * \left\{ \sum_k e^{-\frac{(t-kT_c)^2}{W^2}} C_i(-t) \right\}. \end{aligned} \quad \text{(B10)}$$

In the same manner, the other integrations of (B7) will be derived as following:

$$I_2 = \int_0^{Tc} E\{N_2(t_1,\tau)|t_1\}dt_1 = \frac{\alpha^2 a_d^2}{4}\left\{e^{-\frac{t^2}{W^2}}C_i(t)\right\} * \left\{\sum_k e^{-\frac{(t+T_d-kT_c)^2}{W^2}}C_i(-t)\right\} \tag{B11}$$

$$I_3 = \int_0^{Tc} E\left\{N_3(t_1,\tau)|t_1\right\}dt_1 = \frac{\alpha^2 a_d^2}{4}\left\{e^{-\frac{(t-T_d)^2}{W^2}}C_i(t)\right\} * \left\{\sum_k e^{-\frac{(t-kT_c)^2}{W^2}}C_i(-t)\right\} \tag{B12}$$

$$I_4 = \int_0^{Tc} E\{N_4(t_1,\tau)|t_1\}dt_1 = \frac{\alpha^2 a_d^2}{4}\left\{e^{-\frac{(t-T_d)^2}{W^2}}C_i(t)\right\} * \left\{e^{-\frac{(t+T_d)^2}{W^2}}C_i(-t) + \sum_k e^{-\frac{(t+T_d-kT_c)^2}{W^2}}C_i(-t)\right\}. \tag{B13}$$

The autocorrelation function of $n(t)$, $R_n(\tau)$, can be carried out substituting (B10)–(B13) into (B7). To facilitate the derivation of the Fourier transform of (B10)–(B13), we first derive the following general expressions:

$$\sum_k e^{-\frac{(t-kT_c-\zeta)^2}{W^2}}C_{\rm ph}(-t) = \sum_k e^{-\frac{(t-kT_c-\zeta)^2}{W^2}}\sinh^2\left(\gamma La_c e^{-\frac{(-t-kT_c-\theta)^2}{W^2}}\right) = \sum_{k=-\infty}^{\infty} D_k e^{-jk\omega_c t}. \tag{B14}$$

If $F.T(.)$ denotes the Fourier-transform operation, then we have

$$F.T\left\{\sum_k e^{-\frac{(t-kT_c-\zeta)^2}{W^2}}C_{ph}(-t)\right\} = 2\pi\sum_{k=-\infty}^{\infty} D_k\delta(\omega-k\omega_c) \tag{B15}$$

$$\sum_k e^{-\frac{(t-kT_c-\zeta)^2}{W^2}}C_{\rm par}(-t) = (\gamma La_c)^2\sum_k e^{-\frac{(t-kT_c-\zeta)^2}{W^2}}e^{-2\frac{(-t-kT_c-\theta)^2}{W^2}} = \sum_{k=-\infty}^{\infty} E_k e^{-jk\omega_c t} \tag{B16}$$

$$F.T\left\{\sum_k e^{-\frac{(t-kT_c-\zeta)^2}{W^2}}C_{\rm par}(-t)\right\} = 2\pi\sum_{k=-\infty}^{\infty} E_k\delta(\omega-k\omega_c) \tag{B17}$$

$$F.T\left\{e^{-\frac{(t-\zeta)^2}{W^2}}C_i(t)\right\} = \frac{1}{2\pi}f.t.\left\{e^{-\frac{(t-\zeta)^2}{W^2}}\right\} * f.t.\{C_i(t)\} = \sum_{k=-\infty}^{\infty} F_k W\sqrt{\pi}\exp\left(-\frac{(\omega-k\omega_c)^2W^2}{4} - j(\omega-k\omega_c)\zeta\right) \tag{B18}$$

$$F.T\left\{e^{-\frac{(t-\zeta)^2}{W^2}}C_i(-t)\right\} = \frac{1}{2\pi}f.t.\left\{e^{-\frac{(t-\zeta)^2}{W^2}}\right\} * f.t.\{C_i(-t)\} = \sum_{k=-\infty}^{\infty} F_k^* W\sqrt{\pi}\exp\left(-\frac{(\omega-k\omega_c)^2W^2}{4} - j(\omega-k\omega_c)\zeta\right) \tag{B19}$$

where the Fourier series coefficients are as following:

$$D_k = W\sqrt{\pi}\sum_{l=1}^{\infty}\frac{(2\gamma La_c)^{2l}}{(2l)!\sqrt{2l+1}}\exp \times\left(-\frac{k^2\omega_c^2W^2}{4(2l+1)} - \frac{2l(\zeta+\theta)^2}{W^2(2l+1)} + j\frac{(\zeta-2l\theta)}{2l+1}\right) \tag{B20}$$

$$E_k = W\sqrt{\frac{\pi}{3}}(\gamma La_c)^2\exp\left(-\frac{k^2\omega_c^2W^2}{12} - \frac{2(\zeta+\theta)^2}{3W^2} + j\frac{(\zeta+2\theta)}{3}\right). \tag{B21}$$

$$F_k = \begin{cases} A_k, \text{index}: i = \text{ph} \\ B_k, \text{index}: i = \text{par}. \end{cases}$$

The Fourier transforms of the expressions in (B10)–(B13) and consequently, $R_n(\tau)$ will be obtained using equations (B15)–(B21) and proper values for parameter ζ.

The Fourier transforms of the expressions (B11), (B12), and the second terms of (B10) and (B13) consist of pure delta functions and will be cancelled by the OPLL's loop filter, except the delta functions with respect to DC frequency. So, the PSD of $n(t)$ at DC frequency is derived as following:

$$S_{\rm ph}(0) = \frac{\alpha^2W^2a_d^2}{4T_C}\pi \times\left\{\sum_{k=-\infty}^{\infty}A_k\exp\left(-\frac{k^2\omega_C^2W^2}{4}\right)\sum_{m=-\infty}^{\infty}A_m^* \exp\left(-\frac{m^2\omega_C^2W^2}{4}\right) + \sum_{k=-\infty}^{\infty}A_k\exp \times\left(-\frac{k^2\omega_C^2W^2}{4} + j\omega_C T_d k\right)\sum_{m=-\infty}^{\infty}A_m^*\exp \times\left(-\frac{m^2\omega_C^2W^2}{4} - j\omega_C T_d k\right)\right\} + \bar{n}_{\rm ph}^2\delta(\omega) = \frac{(\alpha W^2 a_d\pi)^2}{32T_C^3}\left\{\left(\sum_{l=1}^{\infty}\frac{(2\gamma La_C)}{(2l)!\sqrt{l}}\left[1+2\sum_{k=1}^{\infty}\right.\right.\right.$$

$$\exp\left(-\frac{k^2\omega_C^2W^2}{4}\left(1+\frac{1}{2l}\right)\right)\cos(k\omega_C\theta)\Bigg]\Bigg)^2 + \left(\sum_{l=1}^{\infty}\frac{(2\gamma La_C)^{2l}}{(2l)!\sqrt{l}}\left[1+2\sum_{k=1}^{\infty}\exp\times\left(-\frac{k^2\omega_C^2W^2}{4}\left(1+\frac{1}{2l}\right)\right)\cos\left(k\omega_C(\theta+T_d)\right)\right]\right)^2\Bigg\} + \bar{n}_{\rm ph}^2\delta(\omega) \quad \text{(B22)}$$

$$S_{\rm par}(0) = \frac{\alpha^2W^2a_d^2}{4T_C}\pi\sum_{k=-\infty}^{\infty}\sum_{m=-\infty}^{\infty}B_kB_m^*\exp\times\left(-\frac{(k^2+m^2)\omega_C^2W^2}{4}\right)\left\{1+e^{j\omega_C T_d(k-m)}\right\} + \bar{n}_{\rm par}^2\delta(\omega) = \frac{(\alpha a_d\pi)^2(\gamma La_CW)^4}{8T_C^3}\sum_{k=-\infty}^{\infty}\sum_{m=-\infty}^{\infty}\exp\left(-\frac{3(k^2+m^2)\omega_C^2W^2}{8}\right)\times\left[e^{j\omega_C(k-m)\theta}+e^{j\omega_C(k-m)(T_d+\theta)}\right] + \bar{n}_{\rm par}^2\delta(\omega)$$

$$= \frac{(\alpha a_d\pi)^2(\gamma La_CW)^4}{4T_C^3}\Bigg\{\Bigg(1+2\sum_{k=1}^{\infty}\exp\left(-\frac{3k^2\omega_C^2W^2}{8}\right)\cos(k\omega_C\theta)\Bigg)^2 + \left(1+2\sum_{k=1}^{\infty}\exp\left(-\frac{3k^2\omega_C^2W^2}{8}\right)\cos\left(k\omega_C(\theta+T_d)\right)\right)^2\Bigg\} + \bar{n}_{\rm par}^2\delta(\omega). \quad \text{(B23)}$$

The delta functions in (B22) and (B23), represent the pure DC power of $n(t)$ and without additional derivations, we can represent their values in terms of DC component of $n(t)$.

REFERENCES

[1] M. Jinno and T. Matsumoto, "All-optical timing extraction using a 1.5 μm self pulsating multielectrode DFB LD," *Electron. Lett.*, vol. 24, pp. 1426–1427, 1988.

[2] P. E. Barnsley, H. J. Wickes, G. E. Wickens, and D. M. Spirit, "All-optical clock recovery from 5 Gb/s RZ data using a self-pulsating 1.56 μm laser diode," *IEEE Photon. Technol. Lett.*, vol. 3, no. 10, pp. 942–945, 1991.

[3] M. Jinno, T. Matsumoto, and M. Koga, "All-optical timing extraction using an optical tank circuit," *IEEE Photon. Technol. Lett.*, vol. 2, no. 3, pp. 203–204, Mar. 1990.

[4] Z. Xiang, L. Chao, S. Ping, H. H. M. Shalaby, T. H. Cheng, and P. Ye, "A performance analysis of an all-optical clock extraction circuit based on Fabry-Perot filter," *J. Lightw. Technol.*, vol. 19, no. 5, pp. 603–613, May 2001.

[5] S. Kawanishi and M. Saruwatari, "New-type phase-locked loop using travelling-wave laser-diode optical amplifier for very high-speed optical transmission," *Electron. Lett.*, vol. 24, pp. 1452–1453, 1988.

[6] S. Kawanishi and M. Saruwatari, "10 GHz timing extraction from randomly modulated optical pulses using phase-locked loop with travelling-wave laser-diode optical amplifier using optical gain modulation," *Electron. Lett.*, vol. 28, pp. 510–511, 1992.

[7] S. Kawanishi and M. Saruwatari, "Ultra-high-speed PLL-type clock recovery circuit based on all-optical gain modulation in traveling-wave laser diode amplifier," *J. Lightw. Technol.*, vol. 11, no. 12, pp. 2123–2129, Dec. 1993.

[8] E. S. Awad, C. J. K. Richardson, P. S. Cho, N. Moulton, and J. Goldhar, "Optical clock recovery using SOA for relative timing extraction between counterpropagating short picosecond pulses," *IEEE Photon. Technol. Lett.*, vol. 14, no. 3, pp. 396–398, Mar. 2002.

[9] H. Bulow, "Optoelectronic synchronisation scheme for ultrahigh-speed optical demultiplexer," *Electron. Lett.*, vol. 31, pp. 1937–1938, 1995.

[10] I. Phillips, A. Gloag, P. Kean, N. Doran, I. Bennion, and A. Ellis, "Simultaneous demultiplexing, data regeneration, and clock recovery with a single semiconductor optical amplifier-based nonlinear-optical loop mirror," *Opt. Lett.*, vol. 22, pp. 1326–1328, 1997.

[11] T. Yamamoto, L. Oxenlowe, C. Schmidt, C. Schubert, E. Hilliger, U. Feiste *et al.*, "Clock recovery from 160 Gbit/s data signals using phase-locked loop with interferometric optical switch based on semiconductor optical amplifier," *Electron. Lett.*, vol. 37, pp. 509–510, 2001.

[12] Y. M. Jhon, H. J. Ki, and S. H. Kim, "Clock recovery from 40 Gbps optical signal with optical phase-locked loop based on a terahertz optical asymmetric demultiplexer," *Opt. Commun.*, vol. 220, pp. 315–319, 2003.

[13] I. Phillips, A. Gloag, D. Moodie, N. Doran, I. Bennion, and A. Ellis, "Simultaneous demultiplexing and clock recovery using a single electroabsorption modulator in a novel bi-directional configuration," *Opt. Commun.*, vol. 150, pp. 101–105, 1998.

[14] I. Phillips, A. Gloag, D. Moodie, N. Doran, I. Bennion, and A. Ellis, "Drop and insert multiplexing with simultaneous clock recovery using an electroabsorption modulator," *IEEE Photon. Technol. Lett.*, vol. 10, no. 2, pp. 291–293, Feb. 1998.

[15] D. T. Tong, B. Mikkelsen, T. Nielsen, K. Dreyer, and J. Johnson, "Optoelectronic phase-locked loop with balanced photodetection for clock recovery in high-speed optical time-division-multiplexed systems," *IEEE Photon. Technol. Lett.*, vol. 12, no. 8, pp. 1064–1066, Aug. 2000.

[16] D. Tong, K.-L. Deng, B. Mikkelsen, G. Raybon, K. Dreyer, and J. Johnson, "160 Gbit/s clock recovery using electroabsorption modulator-based phase-locked loop," *Electron. Lett.*, vol. 36, pp. 1951–1952, 2000.

[17] I. Kang and M. Yan, "Simple setup for simultaneous optical clock recovery and ultra-short sampling pulse generation," *Electron. Lett.*, vol. 38, pp. 1199–1201, 2002.

[18] C. Boerner, C. Schubert, C. Schmidt, E. Hilliger, V. Marembert, J. Berger *et al.*, "160 Gbit/s clock recovery with electro-optical PLL using bidirectionally operated electroabsorption modulator as phase comparator," *Electron. Lett.*, vol. 39, pp. 1071–1073, 2003.

[19] J. Turkiewicz, E. Tangdiongga, G. Khoe, and H. de Waardt, "Clock recovery and demultiplexing performance of 160-Gb/s OTDM field experiments," *IEEE Photon. Technol. Lett.*, vol. 16, no. 6, pp. 1555–1557, Jun. 2004.

[20] H.-F. Chou, Z. Hu, J. E. Bowers, D. J. Blumenthal, K. Nishimura, R. Inohara, and M. Usami, "Simultaneous 160-Gb/s demultiplexing and clock recovery by utilizing microwave harmonic frequencies in a traveling-wave electroabsorption modulator," *IEEE Photon. Technol. Lett.*, vol. 16, no. 2, pp. 608–610, Feb. 2004.

[21] E. S. Awad, P. Cho, N. Moulton, and J. Goldhar, "All-optical timing extraction with simultaneous optical demultiplexing from 40 Gb/s using a single electroabsorption modulator," *IEEE Photon. Technol. Lett.*, vol. 15, no. 1, pp. 126–128, Jan. 2003.

[22] E. S. Awad, P. S. Cho, and J. Goldhar, "Simultaneous four-wave mixing and cross-absorption modulation inside a single EAM for high-speed optical demultiplexing and clock recovery," *IEEE Photon. Technol. Lett.*, vol. 17, no. 7, pp. 1534–1536, Jul. 2005.

[23] E. S. Awad, P. S. Cho, N. Moulton, and J. Goldhar, "Subharmonic optical clock recovery from 160 Gb/s using time-dependent loss saturation inside a single electroabsorption modulator," *IEEE Photon. Technol. Lett.*, vol. 15, no. 12, pp. 1764–1766, Dec. 2003.

[24] E. S. Awad, P. S. Cho, C. Richardson, N. Moulton, and J. Goldhar, "Optical 3R regeneration using a single EAM for all-optical timing extraction with simultaneous reshaping and wavelength conversion," *IEEE Photon. Technol. Lett.*, vol. 14, no. 9, pp. 1378–1380, Sep. 2002.

[25] H. Dong, H. Sun, G. Zhu, Q. Wang, and N. Dutta, "Clock recovery using cascaded LiNbO3 modulator," *Opt. Exp.*, vol. 12, pp. 4751–4757, 2004.

[26] O. Kamatani, S. Kawanishi, and M. Saruwatari, "Prescaled 6.3 GHz clock recovery from 50 Gbit/s TDM optical signal with 50 GHz PLL using

four-wave mixing in a travelling-wave laser diode optical amplifier," *Electron. Lett.*, vol. 30, pp. 807–809, 1994.
[27] O. Kamatani and S. Kawanishi, "Ultrahigh-speed clock recovery with phase lock loop based on four-wave mixing in a traveling-wave laser diode amplifier," *J. Lightw. Technol.*, vol. 14, no. 8, pp. 1757–1767, Aug. 1996.
[28] J. Hansryd, P. A. Andrekson, M. Westlund, J. Li, and P.-O. Hedekvist, "Fiber-based optical parametric amplifiers and their applications," *IEEE J. Sel. Topics Quantum Electron.*, vol. 8, no. 3, pp. 506–520, May/Jun. 2002.
[29] L. Provino, A. Mussot, E. Lantz, T. Sylvestre, and H. Maillotte, "Broadband and flat parametric amplifiers with a multisection dispersion-tailored nonlinear fiber arrangement," *JOSA B*, vol. 20, pp. 1532–1537, 2003.
[30] B. P. Kuo, A. O. J. Wiberg, N. Alic, and S. Radic, "Self-phase tracked fiber-optical parametric sampling gate for 640-Gb/s OTDM de-multiplexing," in *Proc. 36th Eur. Conf. Exhib. Opt. Commun.*, 2010, pp. 1–3.
[31] A. O. J. Wiberg, C.-S. Bres, B. P. Kuo, J. X. Zhao, N. Alic, and S. Radic, "Sampling of multiple 320-Gb/s channels by single parametric gate," *IEEE Photon. Technol. Lett.*, vol. 21, no. 12, pp. 796–798, Jun. 2009.
[32] P. A. Andrekson, "Picosecond optical sampling using four-wave mixing in fibre," *Electron. Lett.*, vol. 27, pp. 1440–1441, 1991.
[33] P. O. Hedekvist, M. Karlsson, and P. A. Andrekson, "Fiber four-wave mixing demultiplexing with inherent parametric amplification," *J. Lightw. Technol.*, vol. 15, no. 11, pp. 2051–2058, Nov. 1997.
[34] X. Feng, F. Poletti, A. Camerlingo, F. Parmigiani, P. Petropoulos, P. Horak *et al.*, "Dispersion controlled highly nonlinear fibers for all-optical processing at telecoms wavelengths," *Opt. Fiber Technol.*, vol. 16, pp. 378–391, Dec. 2010.
[35] G. Agrawal, *Nonlinear Fiber Optics*, 5th ed. Amsterdam, The Netherlands: Elsevier, 2012.
[36] M. E. Marhic, *Fiber Optical Parametric Amplifiers, Oscillators and Related Devices*. Cambridge, U.K.: Cambridge Univ. Press, 2008.
[37] A. J. Viterbi, *Principles of Coherent Communication*, vol. 14. New York, NY, USA: McGraw-Hill, 1966.
[38] F. M. Gardner, *Phaselock Techniques*. Hoboken, NJ, USA: Wiley, 2005.
[39] R. E. Best, *Phase-Locked Loops: Design, Simulation and Applications*. New York, NY, USA: McGraw-Hill, 2003.
[40] H. Zarkoob and J. A. Salehi, "Performance limits of optical clock recovery systems based on two-photon absorption detection scheme," *IEEE J. Sel. Topics Quantum Electron.*, vol. 14, no. 3, pp. 963–971, May/Jun. 2008.
[41] A. Durécu-Legrand, C. Simonneau, D. Bayart, A. Mussot, T. Sylvestre, E. Lantz, and H. Maillotte, "Impact of pump OSNR on noise figure for fiber-optical parametric amplifiers," *IEEE Photon. Technol. Lett.*, vol. 17, no. 6, pp. 1178–1180, Jun. 2005.
[42] P. Kylemark, M. Karlsson, T. Torounidis, and P. A. Andrekson, "Noise statistics in fiber optical parametric amplifiers," *J. Lightw. Technol.*, vol. 25, no. 2, pp. 612–620, Feb. 2007.
[43] Z. Tong, A. Bogris, M. Karlsson, and P. A. Andrekson, "Full characterization of the signal and idler noise figure spectra in single-pumped fiber optical parametric amplifiers," *Opt. Exp.*, vol. 18, pp. 2884–2893, 2010.
[44] R. M. Gagliardi and S. Karp, *Optical Communications*. NewYork, NY, USA: Wiley, 1995.
[45] E. Desurvire, "On the physical origin of the 3-dB noise figure limit in laser and parametric optical amplifiers," *Opt. Fiber Technol.*, vol. 5, pp. 40–61, 1999.

Rasoul Damani was born in Saravan, Iran, on February 23, 1974. He received the B.S. and M.S. degrees from the Sharif University of Technology (SUT), Tehran, Iran, in 1998 and 2000, respectively, all in electrical engineering. He is currently working toward the Ph.D. degree in the Department of Electrical Engineering, SUT. Since 2009, he has been working as a Member of the Optical Networks Research Lab. at SUT. His research interests include the areas of all-optical clock recovery, nonlinear fiber optics, optical CDMA systems, optical amplifiers, and wireless networks.

Jawad A. Salehi (M'84–SM'07–F'10) was born in Kazemain, Iraq, on December 22, 1956. He received the B.S. degree from the University of California, Irvine, CA, USA, in 1979, and the M.S. and Ph.D. degrees from the University of Southern California (USC), Los Angeles, CA, USA, in 1980 and 1984, respectively, all in electrical engineering. He is currently a Full Professor at the Optical Networks Research Laboratory, Department of Electrical Engineering, Sharif University of Technology (SUT), Tehran, Iran, where he is also the Co-Founder of the Advanced Communications Research Institute. From 1981 to 1984, he was a Full-Time Research Assistant at the Communication Science Institute, USC. From 1984 to 1993, he was a Member of Technical Staff of the Applied Research Area, Bell Communications Research, Morristown, NJ, USA. During 1990, he was with the Laboratory of Information and Decision Systems, Massachusetts Institute of Technology, Cambridge, as a Visiting Research Scientist. From 1999 to 2001, he was the Head of the Mobile Communications Systems Group and the Co-Director of the Advanced and Wideband Code-Division Multiple Access (CDMA) Laboratory, Iran Telecom Research Center, Tehran. From 2003 to 2006, he was the Director of the National Center of Excellence in Communications Science, Department of Electrical Engineering, SUT. He is the holder of 12 U.S. patents on optical CDMA. His current research interests include optical multiaccess networks, optical orthogonal codes, fiber-optic CDMA, femtosecond or ultrashort light pulse CDMA, spread-time CDMA, holographic CDMA, wireless indoor optical CDMA, all-optical synchronization, and applications of erbium-doped fiber amplifiers in optical systems. He has been an Associate Editor for Optical CDMA of the IEEE TRANSACTIONS ON COMMUNICATIONS since May 2001. In September 2005, he was elected as the Interim Chair of the IEEE Iran Section. He received several awards including the Bellcore's Award of Excellence, the Nationwide Outstanding Research Award from the Ministry of Science, Research, and Technology in 2003, and the Nation's Highly Cited Researcher Award in 2004. In 2007, he received Khwarazmi International prize, first rank, in fundamental research and also the outstanding Inventor Award (Gold medal) from World Intellectual Property Organization, Geneva, Switzerland. He is among the 250 preeminent and most influential researchers worldwide in the Institute for Scientific Information Highly Cited in the Computer-Science Category. He also received the IEEE's Best Paper Award in 2004 from the International Symposium on Communications and Information Technology, Sapporo, Japan.